Received December 30, 2019, accepted January 9, 2020, date of publication January 14, 2020, date of current version January 23, 2020.

Digital Object Identifier 10.1109/ACCESS.2020.2966496

Investigation on the Parasitic Capacitance of High Frequency and High Voltage Transformers of Multi-Section Windings

LE DENG*, PENGBO WANG*, XIAOFENG LI, HOUXIU XIAO, AND TAO PENG

Wuhan National High Magnetic Field Center, Huazhong University of Science and Technology, Wuhan 430074, China

State Key Laboratory of Advanced Electromagnetic Engineering and Technology, Huazhong University of Science and Technology, Wuhan 430074, China

*(*Le Deng and Pengbo Wang contributed equally to this work.*) Corresponding author: Houxiu Xiao (xiaohouxiu@hust.edu.cn)

This work was supported in part by the National Key Research and Development Program of China under Grant 2016YFA0401703, in part by the Fundamental Research Funds for the Central Universities under Grant 5003132002, and in part by the Fund of the State Key Laboratory of Solidification Processing in NWPU under Grant SKLSP201806.

ABSTRACT Resonant converters are widely used in high voltage applications thanks to the soft switching technologies. The high frequency and high voltage (HFHV) transformer is the most complicated and important part to boost the voltage by tens or hundreds of times, and the parasitic capacitance of the transformers is critical to the performances of resonant converters. To reduce the parasitic capacitance, the multi-section winding technique is usually employed in HFHV transformers. However, the parasitic capacitance values calculated by the classical methods are not consistent with the experimental results of HFHV transformers, and they are usually designed and optimized with low efficiency. This paper proposes a new analytic method for calculating the parasitic capacitance of HFHV transformers of multi-section windings, which is verified with good accuracy by experimental results.

INDEX TERMS HFHV transformer, parasitic capacitance, resonant converters, multi-section windings.

I. INTRODUCTION

High frequency resonant DC-DC converters, which can reduce the switching losses and the system volume, are used more and more widely in high voltage applications [1], [2]. The HFHV transformers are the most challenging and essential components for those converters. The high turn ratio of the HFHV transformers renders a large parasitic inductance or capacitance. At high frequencies, the impacts of parasitic capacitances on harmonic analysis of the HFHV transformer on the converter cannot be ignored. Total parasitic capacitance will generate loop reactive current, and parasitic capacitance between windings is responsible for the electromagnetic interference [3]–[5]. The parasitic capacitance will distort the current waveform and decrease the overall efficiency [6]. Therefore, the parasitic capacitance is regarded as an important performance indicator of HFHV transformers. For an instance, the LC converters (Fig. 1 (a)) are preferred by the chargers of high voltage capacitor banks [2], [7]–[11] because of the characteristics of constant output current and short circuit proof ability. However, the equivalent parasitic capacitance C_p existing in the HFHV transformers makes the LC converter an LCC type in practice. Even for the LCC converter, the C_p is a critical parameter. As shown in Fig. 1(b), the parasitic capacitance C_p decreases remarkably the charging rate and efficiency. It is a fundamental issue to calculate the parasitic capacitance for optimizing the performance or utilizing the parasitic capacitance as constitutive elements of the resonant converters.

Many efforts have been made to model the capacitive effects of HFHV transformers. When the frequency is not very high, the models of lumped parameters focused on winding levels have been established [3]–[6], [12]–[21]. The π-shaped model was widely used [4]–[6], [12], [21]. The six-capacitance model was used to investigate the whole electrostatic behavior of the transformer, where the transformer was regarded as a three-port network considering the third current running between the two windings via parasitic capacitances [13]–[20].

The analytical approach for the parasitic capacitance calculation is usually preferred for the reasons of fast computation and intuitive physical concepts [22]–[24]. According

The associate editor coordinating the review of this manuscript and approving it for publication was Zhilei Yao.

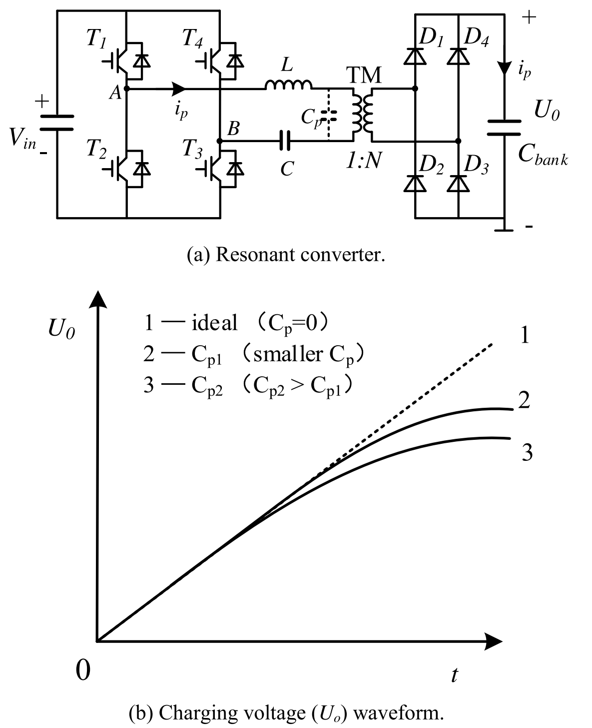

FIGURE 1. The series resonant charger for high voltage capacitor banks.

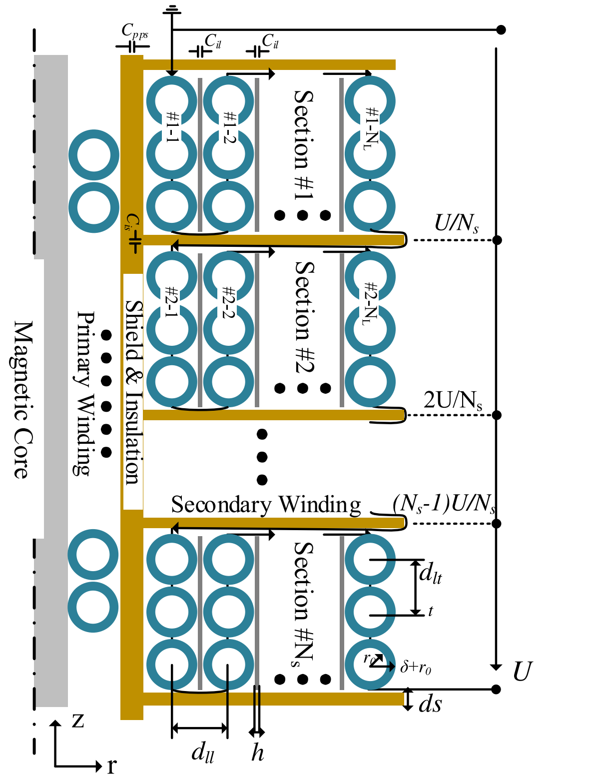

FIGURE 2. Multi-section winding's structure. r_0 is the effective diameter of the Litz wire, δ is insulation thickness of Litz wire, d_{tt} is distance between turns (1.8 mm), d_{ll} is the distance between layers (1.6 mm).

to the equivalent capacitance reflecting law of transformers [13], the parasitic capacitance of the secondary winding (C_s) becomes a predominant part because of the very high turn ratio N. So it usually gets the attention of the analytical approach. Actually, the classical calculation methods of the parasitic capacitance for mono-section windings are fully discussed and reviewed [13], [15], [16], [25]–[28].

However, the multi-section winding technique, whose winding is divided into separate identical sections, is widely used in HFHV transformers to reduce the parasitic capacitance [9], [11], [16]. For high power HFHV transformers of multi-sections, it is usually found that the results of the parasitic capacitance model of mono-section do not match with the experimental results. This is because the high power HFHV transformer has a large turn number of the secondary winding, but the winding space of the magnetic core is also limited. So the intersection capacitance cannot be neglected anymore due to the small section gap. Unfortunately, the intersection parasitic capacitance is rarely discussed in previous works ...[17, 18]. This paper attempt to come up with a more accurate calculation model of the parasitic capacitance of the secondary side of HFHV transformers of multi-section windings.

II. TRANSFORMERS OF MULTI-SECTION WINDINGS

The potential difference between 2 successive layers renders the interlayer parasitic capacitance. In previous literature, the equivalent capacitance is analyzed and calculated by using the law of energy [13], [26]. Analogically, there is also a potential difference between both sides of the section gap, rendering the intersection parasitic capacitance. All the symbols used in this paper are described in Table 1. The multi-section structure is shown in Fig. 2, there are N_s sections of winding connected in the Z-type method, and each section has identical layers and turns winded in the U-type method. There is an insulating layer between each layer and section, so the wires can be arranged in order by fine winding. The disordered arrangement which will not be considered in this paper can be referred to references [13], [16], [29].

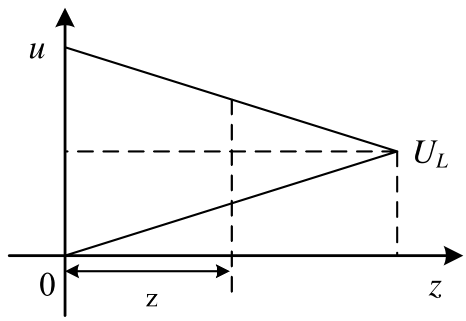

FIGURE 3. The potential distribution between 2 layers.

A. INTERLAYER PARASITIC CAPACITANCE (C1)

The voltage across each layer equals U_L and the winding length for each layer is L_L. Then the voltage difference between 2 layers along the z-axis (as shown in Fig. 3) is

$$V_{LL}(z) = \frac{2U_L}{L_L}(L_L - z) \tag{1}$$

TABLE 1. Symbols' description.

Symbol	Description
U_L	Voltage drop across one layer
L_L	Winding length of each section
N_L	Layer number in each section
N_s	Section number
V_{LL}	Voltage distribution in layers
C_{L0}	Static capacitance between 2 successive layers
C_{ile}	Equivalent interlayer capacitance of 2 successive layers
W	Electric field Energy
C_{isle}	Equivalent interlayer capacitance of one section
U	Total voltage drop of the entire secondary winding
Δu	Voltage difference at the section gap
C_{is0}	Static intersection capacitance
C_{ise}	Equivalent capacitance of one section gap
C_1	Total equivalent interlayer capacitance
C_2	Total equivalent intersection capacitance
C_3	Parasitic capacitance of the fringing effect.
C_s	The total parasitic capacitance of the secondary winding
C_{ps}	Parasitic capacitance between primary and secondary windings
C_0	Static capacitance between primary and secondary windings

The static capacitance between the 2 neighboring layers is C_{L0} [26], [30], [31], and the capacitance per unit length is C_{L0}/L_L, The equivalent interlayer capacitance $C_{ile} = C_{L0}/3$ can be solved by equation (1). There are N_L layers in each section, the effective capacitance for each section C_{isle} can be obtained by using the law of energy:

$$W = \frac{1}{2}(\frac{1}{3}C_{L0})(2U_L)^2)(N_L - 1) = \frac{1}{2}C_{isle}(N_L U_L)^2 \quad (2)$$

And we have $C_{isle} = 4C_{ile}(N_L\text{-}1)/N_L^2$. For N_s sections connected in series, the total effective interlayer capacitance C_1 is

$$C_1 = \frac{C_{ilse}}{N_s} = \frac{1}{N_s}\frac{(N_L - 1)}{N_L^2}\frac{4C_{L0}}{3} \quad (3)$$

The formula (3) is used to calculate the parasitic capacitance of multi-section windings in the classical methods [13], [31].

B. INTERSECTION PARASITIC CAPACITANCE (C_2)

The potential distribution at the section gap is analogous to the case of interlayer. The voltage distribution at the section gap between #1 and #2, which are similar to Z-type winding in [11], [13], [16], can be seen in Fig. 4. The potential at the down end (the upside of the section gap) of #1-1 and #1-2 layers are both U_L. So the potential of the upside of the section gap begins with U_L and increases by the step of $2U_L$ in every 2 layers. Similarly, the potential of the downside of the section gap begins with U/N_s and increases by the step of $2U_L$ in every 2 layers.

Assuming the voltage drop across the entire secondary winding is U and the layer number $N_L \gg 1$, $U_L = U/(N_s N_L) \ll U/N_s$, the voltage $u(r)$ will distribute linearly along r direction [13], [31]. And the voltage difference is $\Delta u(r) \approx U/N_s$. Suppose the static capacitance of the section

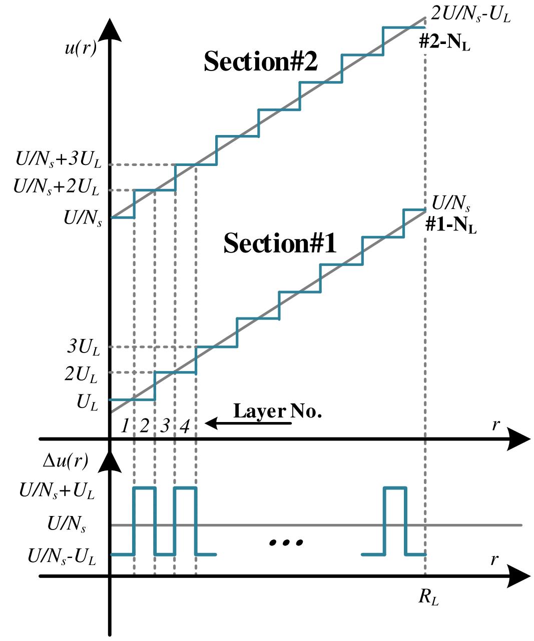

FIGURE 4. Voltage distribution at the section gap.

gap is C_{is0}, the corresponding equivalent capacitance is C_{ise}, and $\Delta u = U/N_s$, we have

$$W = \frac{1}{2}C_{is0}(\Delta u)^2(N_s - 1) = \frac{1}{2}C_{ise}(\frac{2U}{N_s})^2 \quad (4)$$

It results in equivalent capacitance $C_{ise} = C_{is0}/4$. There are $N_s - 1$ identical section gaps. The equivalent capacitance of all intersection capacitance C_2 can be solved by using the law of energy conservation:

$$W_t = \frac{1}{2}C_2 U^2 = \frac{1}{2}C_{ise}(\frac{2U}{N_s})^2(N_s - 1) \quad (5)$$

Then we have $C_2 = 4(N_s - 1)C_{ise}/N_s^2$, and

$$C_2 = \frac{(N_s - 1)}{N_s^2}C_{is0} \quad (6)$$

where N_s is the number of sections, $C_{is0} = \varepsilon S_s/d$, ε is the permittivity of the filling material between the section gap, d is the length of the gap, S_s is the area of the secondary winding in radial section.

C. PARASITIC CAPACITANCE CAUSED BY THE FRINGING FIELD (C_3)

The COMSOL Multiphysics analyzed results of multi-section windings (in the axial symmetry model) are shown in Fig. 5 (a). The stray electric field exists around the transformer's windings due to the potential difference along the z-direction, which is known as the fringing effect. The fringing effect is usually ignored, but it has to be considered for a more accurate model. Besides, the results also show that the electric field intensity at the section gap is significant indeed that renders the intersection capacitance C_3.

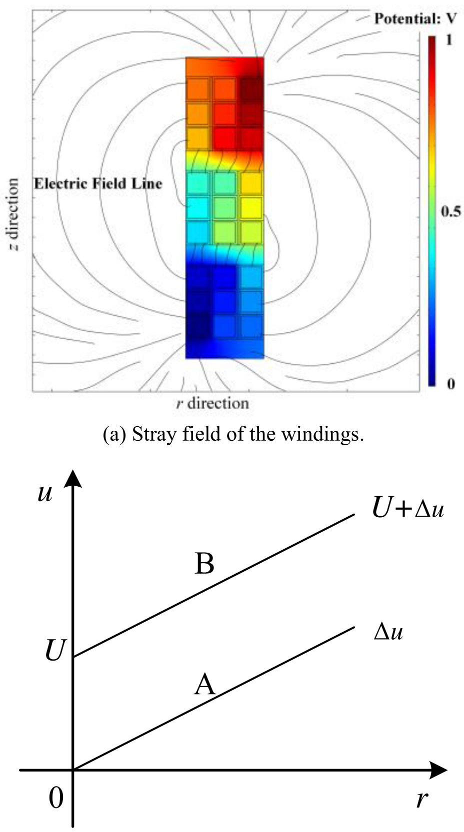

(a) Stray field of the windings.

(b) Potential distribution of top/bottom windings.

FIGURE 5. **Fringing effect of the windings.**

The fringing effect of the plate capacitor is already discussed in [24], [30]–[32] and some analytical solutions of the capacitance are proposed [31]. As shown in Fig. 5, the electric potential increases linearly along z-direction that is analogous to the potential distribution of the plate capacitor. So the electric field distributions in the air are similar to each other.

As shown in Fig. 5 (b), although the potential of the bottom or top windings increases along r-direction, the potential difference between them along r-direction is constant. So the capacitance of the fringing field of the transformer's windings can be estimated as a plate capacitor. Considering the proportion of fringing effect capacitance being minor in the transformer, a concise analytical estimating of fringing effect capacitance C_3 [31] is available.

$$C_3 = 0.65\varepsilon_0 D \qquad D = \begin{cases} 2a + 2b + 4w \\ \pi(R_1 + R_2) \end{cases} \tag{7}$$

where ε_0 is the dielectric constant of air, D is the mid-diameter of the wingdings. In our transformers, D is the average turn length in one section. When the shape of the winding's skeleton in the radial section is a rectangle with lengths of a and b,

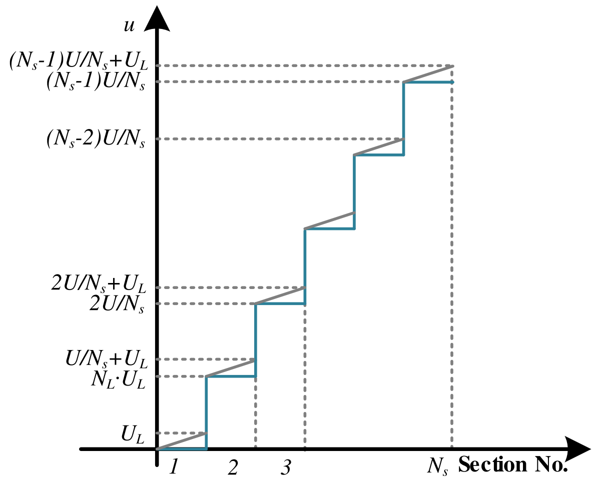

FIGURE 6. **Voltage distribution of the inner layer of the secondary winding.**

and the thickness of the winding is w, $D = 2a+2b+4w$; When the shape is a cylinder with inner radius R_1 and outer radius R_2, $D = \pi(R_1 + R_2)$.

The total parasitic capacitance of the secondary windings C_s can be obtained by summing up the interlayer capacitance (equation (3)), intersection capacitance (equation (6)) and the fringing effect capacitance (equation (7)),

$$C_s = C_1 + C_2 + C_3 \tag{8}$$

D. PARASUTIC CAPACITANCE BETWEEN PRIMARY AND SECONDARY WINDINGS (C_{ps})

For a transformer with a large turn ratio, the voltage of the secondary winding is much larger than the voltage of the primary winding, so the primary winding can be regarded as zero potential. The voltage distribution of the inner layer of the secondary winding is shown in Fig. 6. For the reasons of $U/N_s \gg U_L$, the voltage distribution can be equivalent to the stepped distribution shown as the blue line. Then the capacitance between primary and secondary windings C_{ps} can be obtained via the integration of voltage [33]:

$$\frac{1}{2}C_{ps}U^2 = \int_0^{N_s} \frac{1}{2}\frac{C_0}{N_s}\left[(n-1)\frac{U}{N_s}\right]^2 dn$$
$$\Rightarrow C_{ps} = \frac{C_0}{3}\frac{N_s^2 - 3N_s + 3}{N_s^2} \tag{9}$$

where C_0 is the static capacitance between primary and secondary windings.

According to the equivalent capacitance reflecting law of transformers, the capacitance of the primary winding is neglected because of the high turn ratio. And the total capacitance can be expressed as:

$$C_p = N^2 C_s + NC_{ps} \tag{10}$$

TABLE 2. Calculated results of the transformers in reference [16].

TM	Winding structure[16]	c_s in reference [16] (pF)	Classical method[16]		COMSOL		Formula (8)	
			Value(pF)	error	Value (pF)	error	Value (pF)	error
Transformer#1	Whole winding @ 10mm air section gap	3.84	3.15	-18.0%	3.9	1.5 %	4.20 (C_1=3.15, C_2=0.11, C_3=0.94)	9.4%
Transformer #2	Whole winding @ 17mm air section gap	4.84	3.97	-17.9%	4.57	-5.6 %	5.16 (C_1=3.97, C_2=0.05, C_3=1.14)	6.6%
Transformer #3	Whole winding @ 4mm air section gap	12.80	10.47	-18.2%	12.26	-4.2 %	12.30 (C_1=10.46, C_2=0.35, C_3=1.45)	-3.9%

TABLE 3. Main information of the 6 HFHV transformers.

Transformers	TM #1	TM #2	TM #3	TM #4	TM #5	TM#6
Turn ratio	10/546	10/525	10/324	10/360	10/468	10/468
Secondary winding (Turns × layers ×sections)	14×13 ×3	5×21×5	4×9×9	4×9×10	4 ×9 ×13	3×12 ×13
Winding skeleton size ($width_1$×$width_2$×length) (mm)	49×61×120	61×71×135	45×55×150	40×50×110	80×90×140	80×90×140
Section breath (mm)	25.2	9	8	8	8	6
Winding thickness (mm)	21	34	15	15	15	20
Section gap	6 mm paper tape	3mm G10	3mm G10	2mm G10	3mm G10	4mm G10
Transformers	TM #1	TM #2	TM #3	TM #4	TM #5	TM#6

III. FEM RESULTS, ANALYTICAL RESULTS, AND EXPERIMENTAL RESULTS

First of all, the wingdings structure and the measured values in reference [16] are used to verify the proposed method. Because of the limited structure parameters of the transformers in reference [16], the formula (8) is used to calculate the parasitic capacitance of the secondary windings. Additionally, the COMSOL is also employed to compute the capacitance as well. All the results are listed in Table 2.

It shows 1) the COMSOL and the proposed method are consistent well with each other; 2) the proposed method has better accuracy than the classical method of which the parasitic capacitance parts of C_2 and C_3 are not considered. The error of the proposed method comparing with the measured capacitance is 9.4% (18.0% by using the classical method).

According to reference [16], the outer diameters of the secondary wires of the three transformers are 0.472mm, 0.297mm, and 0.194mm in sequence. And their section breaths are 2.5 mm, 4 mm, and 5 mm in sequence. The section gaps are much larger than or almost equal to the corresponding section breaths. So the intersection capacitance C_2 is minor. The classical method seems still available when the interlayer capacitance C_1 is dominated.

However, in our high voltage (20 kV) and high power application (20 kW), the required space of the secondary windings is much larger because of the larger wire diameter and turn number. The intersection gap is usually limited as listed in Table 3. The high power HFHV transformer is shown in Fig. 7. The secondary windings are made of Litz wire of 1.6 mm diameter, which is made of 150 copper filaments of 0.1 mm diameter [13], [16]. The Litz wire is covered with $\delta = 0.1$ mm Teflon ($\varepsilon_r = 2.55$) insulation. The layer insulation is Kapton film ($\varepsilon_r = 3$) of $h = 0.1$ mm $\sim$ 0.3 mm. And the section gap insulation is filled with insulation paper tape ($\varepsilon_r = 4$) or G10 plate ($\varepsilon_r = 2.5$). The insulation of the primary and secondary windings is with air and Kapton film of 10 mm thickness. The specifications of the 6 transformers are listed in Table 3.


TM #1 (3 sections) TM #5 with G10 gap (13 section)

FIGURE 7. HFHV transformers of multi-section windings.

The calculated results of C_s using the classic methods, COMSOL and the formula (10) proposed in this paper are listed in Table 4. The influence of the core is negligible when the winding is far from the core or a screen is employed [16]. The iron cores are removed to measure the parasitic capacitances of the secondary windings directly. And their parasitic capacitances can be measured by using the frequency resonance point method proposed in [4], [14], [27], [34], [35]. As shown in Fig. 8, the impedance frequency characteristics of the secondary's windings and their inductances are measured by the HIOKI IM-3536 LCR meter. All the measured results are listed in Table 4.

When the section gap is smaller and the windings' thickness is larger in a compact high power HFHV transformer, the classical method may not be available anymore as shown

TABLE 4. Measured and calculated results of the 6 HFHV transformers.

Transformer	Winding structure	Measured c_p (nF)	Classical method (nF)		COMSOL (nF)		Formula (10) (nF)	
			value	error	value	error	value	error
TM #1 (3 section)	Section #1	93.3	82.8	-11.2%	85.3	-8.6%	88.8	-4.8%
	All sections @ 6mm paper section gap	60.2	27.7	-54.4%	55.7	-7.5%	58.5	-2.8%
TM #2 (5 sections)	@ 3mm G10 section gap	68.6	17.4	-74.7%	66.2	-3.5%	66.0	-3.8%
	@ 3 mm air section gap	36.1	17.4	-51.9%	34.7	-3.9%	37.8	4.7%
	@ 10 mm air section gap	27.6	17.4	-40.0%	26.2	-5.1%	29.3	6.2%
TM #3 (9 sections)	@ 3.2mm G10 section gap	4.4	0.9	-79.5%	4.8	9.1%	4.7	6.8%
TM#4 (10 sections)	@ 2mm G10 section gap	9.8	1.4	-85.7%	9.2	-6.1%	9.6	-2.0%
TM #5 (13 sections)	Turn=4, Layer=9 @ 3mm G10 section gap	25.8	6.4	-75.2%	23.4	-9.3%	27.3	5.8%
TM #6 (13 sections)	Turn=3, Layer=12 @ 4 mm G10 section gap	19.4	3.2	-83.5%	18.6	-4.1%	19.1	-1.5%

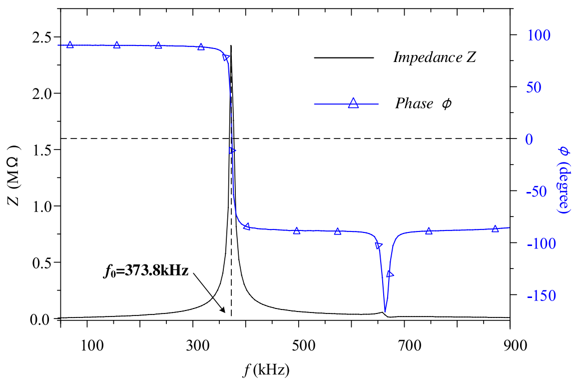

FIGURE 8. Typical impedance frequency characteristics (TM # 2 @ 3mm air gap).

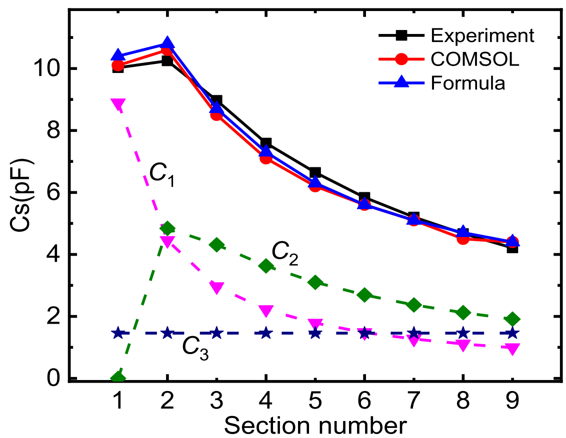

FIGURE 9. C_s varies with the section number (TM #3).

in Table 4. Take transformer TM #2 as an example, the measured C_p (27.6 nF) is still much larger than the classical method prediction (17.4 nF) even when the air section gap is 10 mm. That is because the intersection capacitance cannot be neglected. The existence of the intersection capacitance is also verified by the experimental results of TM #2 with different kinds of section gaps. If the 3 mm G10 ($\varepsilon_r = 2.5$) section gap is replaced by a 3 mm air ($\varepsilon_r = 1$) gap, the total C_p decreases from 68.6 nF to 36.1 nF. But the intersection capacitance is never discussed before. And more sections will make smaller C_p in the traditional idea. That may misguide the design of high power HFHV transformers. With the error smaller than ±7 %, the proposed method considering the intersection capacitance and fringing effect is more accurate. A smaller error is usually limited by the handmade windings and imprecise structure sizes.

Another interesting experiment is carried out on the secondary winding of the transformer TM #3. The parasitic capacitance C_s is measured when the sections are added one by one as shown in Fig. 9. And the values of C_1, C_2, and C_3 of formula (8) are also plotted as dot lines in Fig. 9. The total parasitic capacitance C_s = 10.3 pF for the case of 2 sections, which is not 5 pF as expected by the classical method (C_1) due to the intersection capacitance C_2 (5.3 pF). Also thanks to C_2, C_s does not decrease as rapidly as the prediction of the classical method when the section number increases. The fringing capacitance C_3 is only proportional to the average turn length D. It is independent on section number and remains constant. All the results of the proposed method show a good agreement with the experimental results and the COMSOL results.

The following conclusions can be drawn from above:

- The classic method is valid and accurate to calculate the C_p when it is mono-section windings or multi-windings with large enough section gaps.
- For high power HFHV transformers, the capacitance of the section gaps usually has significant effects on the total C_p value, and it cannot be neglected. Using the classical method may cause big errors.
- The proposed method, taking the section gap parasitic capacitance and fringing effect into account, is valid to calculate the parasitic capacitance of any multi-section windings.

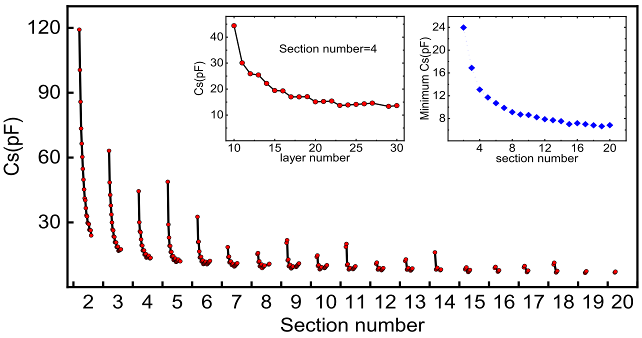

(a) C_s varies with the section & layer number.

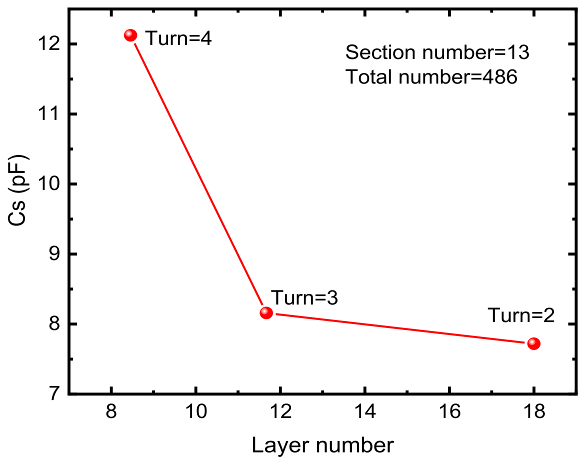

(b) C_s varies with layer number at 13 sections.

FIGURE 10. Optimization analysis of HFHV transformers.

IV. DISCUSSION AND EXPERIMENTAL VERIFICATION

In practice, the parasitic capacitance of the secondary winding becomes a predominant part because of the very high turn ratio. It is interesting and meaningful to know the windings structure that has the minimum parasitic capacitance of the secondary winding C_s. Take the TM #5 transformer in Table 4 as an example, the secondary winding is around 450 turns. All the possible combinations of sections, layers, and turns are tried within the available winding space (the skeleton size or the iron core's window size), and the results are shown in Fig. 9. The section number ranges from 1 to 20. The layer number varies within each section independently. The turn number is determined by the product of the section number and layer number to have the total turn number being constant. All sections are distributed evenly on the skeleton to have a section gap as larger as possible. As shown in Fig. 10 (a), the C_s value decreases remarkably with the section number. For a certain section number, the C_s value also decreases with layer number as shown in the left insert windows of Fig. 10 (a) (4 sections). The right insert windows of Fig. 10 (a) shows the minimum value of C_s for each section number. It follows that the C_s cannot be minimized remarkably by increasing section number after the section is greater than 10. The transformer of 13 sections is chosen, and more details are shown in Fig. 10 (b). The optimized result is

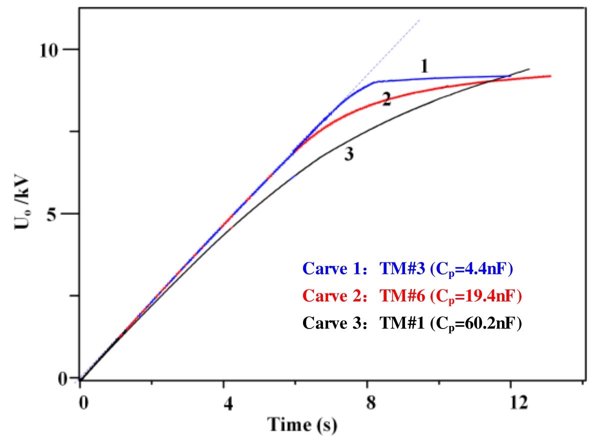

FIGURE 11. Experimental results of the High voltage charger equipped with 3 different transformers.

the structure of 2 turns, 18 layers, and 13 sections. But it is hard to be manufactured. Instead, the other two structures are manufactured, and the results are listed in Table 4.

Three representative transformers in Table 4 are tested by experiments to verify the proposed method: TM #1 (C_p = 60.2 nF, 20 kV rated), TM #3 (C_p = 4.4 nF, 10 kV rated), TM #6 (C_p = 19.4 nF, 20 kV rated). They are tested in a high voltage resonant charger (resonant capacitor C_r = 0.65 μF, f_s = 2.5 kHz). The high capacitance bank to be charged is 165 μF (20 kV rated). The experimental results, as shown in Fig. 11, show that the performance of the LCC converter charger is sensitive to C_p. By using the concept of $i = C(du/dt)$, we know that the performance of the three transformers: TM #3 > TM #6 >TM #1, and the performance of transformer TM #3 is very close to that of an ideal LC resonant converter. Transformer TM #1 is not suitable to be used in an LC resonant converter. The charging current is not constant and decays all the time. On the other hand, it also can be concluded that controlling the parasitic capacitance of the secondary winding is very necessary and challenging for high turn ratio transformers. To design and manufacture a 10 kV rated high power HFHV transformer may be easy. But the difficulty is exponentially growing as the rated voltage rising.

V. CONCLUSION

HFHV transformers are the key and most challenging parts of high voltage converters, and the parasitic capacitance is a critical performance indicator for the HFHV transformers (especially used in high voltage chargers). Many papers are already published on this important issue, where the interlayer capacitance is fully and clearly discussed. But it causes some errors for high power HFHV transformers with multi-section windings. A valid and effective method to calculate the parasitic capacitance, which is verified by the experimental results, is proposed in this paper. The idea of minimizing the parasitic capacitance by increasing the section number is also discussed. For a given winding space, more section number and more layer number (larger section gaps) will gain smaller C_s. But it also shows that excessive section numbers will not gain much smaller C_s value.

ACKNOWLEDGMENT

(Le Deng and Pengbo Wang contributed equally to this work.)

REFERENCES

[1] J. A. Martin-Ramos, A. M. Pernia, J. Diaz, F. Nuno, and J. A. Martinez, ''Power supply for a high-voltage application,'' *IEEE Trans. Power Electron.*, vol. 23, no. 4, pp. 1608–1619, Jul. 2008, doi: 10.1109/TPEL.2008.925153.

[2] H. J. Ryoo, S. R. Jang, Y. S. Jin, J. S. Kim, Y. B. Kim, S. H. Ahn, J. W. Gong, B. H. Lee, and D. H. Kim, ''Design of high voltage capacitor charger with improved efficiency, power density and reliability,'' *IEEE Trans. Dielectr. Electr. Insul.*, vol. 20, no. 4, pp. 1076–1084, Aug. 2013, doi: 10.1109/tdei.2013.6571420.

[3] C. Liu, L. Qi, X. Cui, Z. Shen, and X. Wei, ''Wideband mechanism model and parameter extracting for high-power high-voltage high-frequency transformers,'' *IEEE Trans. Power Electron.*, vol. 31, no. 5, pp. 3444–3455, May 2016, doi: 10.1109/tpel.2015.2464722.

[4] H. Yan Lu, J. Guo Zhu, and S. Hui, ''Experimental determination of stray capacitances in high frequency transformers,'' *IEEE Trans. Power Electron.*, vol. 18, no. 5, pp. 1105–1112, Sep. 2003, doi: 10.1109/tpel.2003.816186.

[5] K. L. Kaiser, *Electromagnetic Compatibility Handbook*. Boca Raton, FL, USA: CRC Press, 2005.

[6] M. Borage, K. Nagesh, M. Bhatia, and S. Tiwari, ''Design of LCL-T resonant converter including the effect of transformer winding capacitance,'' *IEEE Trans. Ind. Electron.*, vol. 56, no. 5, pp. 1420–1427, May 2009, doi: 10.1109/tie.2009.2012417.

[7] S.-R. Jang, H.-J. Ryoo, S.-H. Ahn, J. Kim, and G. H. Rim, ''Development and optimization of high-voltage power supply system for industrial magnetron,'' *IEEE Trans. Ind. Electron.*, vol. 59, no. 3, pp. 1453–1461, Mar. 2012, doi: 10.1109/tie.2011.2163915.

[8] R. Newsom, W. Dillard, and R. Nelms, ''Digital power-factor correction for a capacitor-charging power supply,'' *IEEE Trans. Ind. Electron.*, vol. 49, no. 5, pp. 1146–1153, Oct. 2002, doi: 10.1109/tie.2002.803240.

[9] Y. Gao, K. Liu, Y. Sun, D. Zhang, and P. Yan, ''Design and implementation of a 100 kV bipolar capacitor charger for the aging test of high-voltage switch,'' in *Proc. IEEE Int. Power Modulator High Voltage Conf. (IPMHVC)*, Jun. 2012, doi: 10.1109/ipmhvc.2012.6518836.

[10] M. Jaritz, S. Blume, D. Leuenberger, and J. Biela, ''Experimental validation of a series parallel resonant converter model for a solid state 115-kV long pulse modulator,'' *IEEE Trans. Plasma Sci.*, vol. 43, no. 10, pp. 3392–3398, Oct. 2015, doi: 10.1109/tps.2015.2390258.

[11] P. Thummala, H. Schneider, Z. Zhang, and M. A. E. Andersen, ''Investigation of transformer winding architectures for high-voltage (2.5 kV) capacitor charging and discharging applications,'' *IEEE Trans. Power Electron.*, vol. 31, no. 8, pp. 5786–5796, Aug. 2016, doi: 10.1109/tpel.2015.2491638.

[12] W. Shen, F. Wang, D. Boroyevich, and C. W. Tipton Iv, ''High-density nanocrystalline core transformer for high-power high-frequency resonant converter,'' *IEEE Trans. Ind. Appl.*, vol. 44, no. 1, pp. 213–222, 2008, doi: 10.1109/tia.2007.912726.

[13] J. Biela and J. W. Kolar, ''Using transformer parasitics for resonant converters—A review of the calculation of the stray capacitance of transformers,'' *IEEE Trans. Ind. Appl.*, vol. 44, no. 1, pp. 223–233, Oct. 2008, doi: 10.1109/tia.2007.912722.

[14] B. Cogiore, J. Keradec, and J. Barbaroux, ''The two winding ferrite core transformer: An experimental method to obtain a wide frequency range equivalent circuit,'' in *Proc. IEEE Instrum. Meas. Technol. Conf.*, Dec. 2002, pp. 558–562, doi: 10.1109/imtc.1993.382580.

[15] F. Blache, J.-P. Keradec, and B. Cogitore, ''Stray capacitances of two winding transformers: Equivalent circuit, measurements, calculation and lowering,'' in *Proc. IEEE Ind. Appl. Soc. Annu. Meeting*, Dec. 2002, pp. 1211–1217, doi: 10.1109/ias.1994.377552.

[16] L. Dalessandro, F. Da Silveira Cavalcante, and J. W. Kolar, ''Self-capacitance of high-voltage transformers,'' *IEEE Trans. Power Electron.*, vol. 22, no. 5, pp. 2081–2092, Sep. 2007, doi: 10.1109/tpel.2007.904252.

[17] Z. De Greve, O. Deblecker, and J. Lobry, ''Numerical modeling of capacitive effects in HF multiwinding transformers—Part I: A rigorous formalism based on the electrostatic equations,'' *IEEE Trans. Magn.*, vol. 49, no. 5, pp. 2017–2020, May 2013, doi: 10.1109/tmag.2013.2243421.

[18] Z. De Greve, O. Deblecker, and J. Lobry, ''Numerical modeling of capacitive effects in HF multiwinding transformers—Part II: Identification using the finite-element method,'' *IEEE Trans. Magn.*, vol. 49, no. 5, pp. 2021–2024, May 2013, doi: 10.1109/tmag.2013.2243422.

[19] R. Asensi, R. Prieto, J. A. Cobos, and J. Uceda, ''Modeling high-frequency multiwinding magnetic components using finite-element analysis,'' *IEEE Trans. Magn.*, vol. 43, no. 10, pp. 3840–3850, Oct. 2007, doi: 10.1109/tmag.2007.903162.

[20] A. Schellmanns, K. Berrouche, and J.-P. Keradec, ''Multiwinding transformers: A successive refinement method to characterize a general equivalent circuit,'' *IEEE Trans. Instrum. Meas.*, vol. 47, no. 5, pp. 1316–1321, 1998, doi: 10.1109/19.746603.

[21] S. S. Baek, B. Cougo, S. Bhattacharya, and G. Ortiz, ''Accurate equivalent circuit modeling of a medium-voltage and high-frequency coaxial winding DC-link transformer for solid state transformer applications,'' in *Proc. IEEE Energy Convers. Congr. Expo. (ECCE)*, Sep. 2012, pp. 1439–1446, doi: 10.1109/ecce.2012.6342645.

[22] A. Schellmanns, J.-P. Keradec, J.-L. Schanen, and K. Berrouche, ''Representing electrical behaviour of transformers by lumped element circuits: A global physical approach,'' in *Proc. Conf. Rec. IEEE Ind. Appl. Conf. 34th IAS Annu. Meeting*, Jan. 2003, pp. 2100–2107, doi: 10.1109/ias.1999.806025.

[23] R. Yang, H. Ding, Y. Xu, L. Yao, and Y. Xiang, ''An analytical steady-state model of LCC type series-parallel resonant converter with capacitive output filter,'' *IEEE Trans. Power Electron.*, vol. 29, no. 1, pp. 328–338, Jan. 2014, doi: 10.1109/TPEL.2013.2248753.

[24] W. Chang, ''Analytical IC metal-line capacitance formulas (short papers),'' *IEEE Trans. Microw. Theory Techn.*, vol. MTT-24, no. 9, pp. 608–611, Sep. 1976, doi: 10.1109/tmtt.1976.1128917.

[25] E. Laveuve, J.-P. Keradec, and M. Bensoam, ''Electrostatic of wound components: Analytical results, simulation and experimental validation of the parasitic capacitance,'' in *Proc. Conf. Rec. IEEE Ind. Appl. Soc. Annu. Meeting*, vol. 2, 1991, pp. 1469–1475, doi: 10.1109/ias.1991.178054.

[26] T. Duerbaum and G. Sauerlaender, ''Energy based capacitance model for magnetic devices,'' in *Proc. 16th Annu. IEEE Appl. Power Electron. Conf. Expo. (APEC)*, vol. 1, Nov. 2002, pp. 109–115, doi: 10.1109/apec.2001.911635.

[27] G. Aristoy, A. Santos, and D. Slomovitz, ''Testing methods for measuring the effects of stray capacitances on high-voltage current transformers,'' *IEEE Trans. Instrum. Meas.*, vol. 64, no. 8, pp. 2200–2207, Aug. 2015, doi: 10.1109/tim.2015.2393395.

[28] G. Grandi, M. Kazimierczuk, A. Massarini, and U. Reggiani, ''Stray capacitances of single-layer solenoid air-core inductors,'' *IEEE Trans. Ind. Appl.*, vol. 35, no. 5, pp. 1162–1168, 1999, doi: 10.1109/28.793378.

[29] A. Massarini and M. Kazimierczuk, ''Self-capacitance of inductors,'' *IEEE Trans. Power Electron.*, vol. 12, no. 4, pp. 671–676, Jul. 1997, doi: 10.1109/63.602562.

[30] H. B. Palmer, ''The capacitance of a parallel-plate capacitor by the Schwartz-Christoffel transformation,'' *Electr. Eng.*, vol. 56, no. 3, pp. 363–368, Mar. 1937, doi: 10.1109/ee.1937.6540485.

[31] P. Osterberg and S. Senturia, ''M-TEST: A test chip for MEMS material property measurement using electrostatically actuated test structures,'' *J. Microelectromech. Syst.*, vol. 6, no. 2, pp. 107–118, Jun. 1997, doi: 10.1109/84.585788.

[32] T. Sakurai and K. Tamaru, ''Simple formulas for two- and three-dimensional capacitances,'' *IEEE Trans. Electron Devices*, vol. 30, no. 2, pp. 183–185, Feb. 1983, doi: 10.1109/t-ed.1983.21093.

[33] J. Dong, W. Chen, and Z. Lu, ''Modeling and analysis of capacitive effects in high-frequency transformer of SMPS,'' *Proc. CSEE*, vol. 27, no. 31, pp. 121–126, Nov. 2007.

[34] M. B. Shadmand and R. S. Balog, ''A finite-element analysis approach to determine the parasitic capacitances of high-frequency multiwinding transformers for photovoltaic inverters,'' in *Proc. IEEE Power Energy Conf. Illinois (PECI)*, Feb. 2013, pp. 114–119, doi: 10.1109/peci.2013.6506044.

[35] J. Lou, Y. Chen, D. Liang, L. Gao, F. Dang, and F. Jiao, ''Novel network model for dynamic stray capacitance analysis of planar inductor with nanocrystal magnetic core in high frequency,'' in *Dig. 14th Biennial IEEE Conf. Electromagn. Field Comput.*, May 2010, doi: 10.1109/cefc.2010.5481497.

LE DENG was born in Loudi, Hunan, China, in 1991. She received the B.S. degree in electrical and electronics engineering from the Huazhong University of Science and Technology, Wuhan, China, in 2014, where she is currently pursuing the Ph.D. degree with the Wuhan High Magnetic Field Center.

Her principal research interests include the calculation of parasitic parameters and structural optimization in high-frequency high-voltage transformers.

PENGBO WANG was born in Meishan, Sichuan, China, in 1994. He received the B.S. degree in electrical engineering from Chongqing University, Chongqing, China, in 2017. He is currently pursuing the Ph.D. degree with the Wuhan High Magnetic Field Center, Huazhong University of Science and Technology, Wuhan, China.

His principal research interests include pulsed power technology, terahertz technology, and high-magnetic field technology.

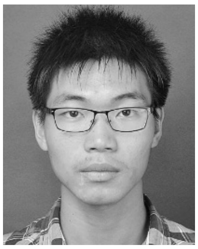

XIAOFENG LI was born in Quanzhou, Fujian, China, in 1994. He received the B.S. degree in electrical engineering and automation from the Huazhong University of Science and Technology, Wuhan, China, in 2017, where he is currently pursuing the M.S. degree with the Wuhan High Magnetic Field Center.

His principal research interests include the high-magnetic field technology and pulse power technology.

HOUXIU XIAO was born in Xishui, Hubei, China, in 1981. He received the B.S. and Ph.D. degrees in electrical and electronics engineering from the Huazhong University of Science and Technology, Wuhan, China, in 2004 and 2006, respectively.

From 2010 to 2011, he worked as a Postdoctoral Researcher with the Laboratoire National des Champs Magnétiques Intenses, CNRS, Grenoble, France. Since 2011, he has been working with the Wuhan National High Magnetic Field Center. He is also a Faculty Member of the Huazhong University of Science and Technology, China. His principal research interests include the high-magnetic field technology, pulse power technology, and terahertz technology.

TAO PENG was born in Hongan, Hubei, China, in 1977. He received the B.S. and Ph.D. degrees in electrical and electronics engineering from the Huazhong University of Science and Technology, Wuhan, China, in 2000 and 2005, respectively.

Since 2005, he has been working with the Wuhan National High Magnetic Field Center. He is also a Faculty Member of the Huazhong University of Science and Technology, China. His principal research interests include the analysis and numerical simulation of electromagnetic field, and generation and application of high magnetic field technology.